Recent results on the scattering of muons on nuclear targets from the E665 experiment

Wolfgang Wittek

Max-Planck-Institut für Physik
München, Germany
(respresenting the E665 collaboration)

Abstract

Nuclear shadowing and diffractive scattering are measured in the interaction of muons on different targets. The size of the shadowing effect and the cross section for coherent diffractive production exhibit a similar dependence on x_{Bj} and the atomic mass A, suggesting a close relation between the two. The nuclear transparency for incoherent diffractive production of $\rho(770)$ mesons increases with Q^2, which may be interpreted as evidence for the onset of color transparency

Résumé

L'effet d'écrantage nucléaire et la diffusion diffractive sont mesurés dans l'interaction de muons avec différentes cibles. L'ampleur de l'effet d'écrantage et la section efficace pour la production cohérente diffractive montrent une dépendance similaire de x_{Bj} et de la masse atomique A, suggérant une relation étroite entre les deux. La transparence nucléaire pour la production incohérente diffractive de mésons $\rho(770)$ augmente avec Q^2, ce qui pourrait être interprété comme preuve pour le début de la transparence de couleur.

1. Introduction

This paper reports results on

- nuclear shadowing,
- diffractive scattering and the
- A-dependence of diffractive ρ production

in inelastic scattering of positive muons on H, D, C, Ca and Pb nuclei at low x_{Bj}. The data were obtained in the fixed-target experiment E665 at the Tevatron at Fermilab. The average beam energy was 470 GeV. Details of the detector and the triggers are described elsewhere [1].

The E665 experiment covers the kinematic region $0.0001 \lesssim x_{Bj} \lesssim 0.2$, at Q^2 values between 0.1 and 10 GeV^2 and ν values of 20 to 400 GeV.

2. Nuclear shadowing

In various lepton nucleus experiments [2, 3] it was found that at low x_{Bj} the cross section σ_A on a nucleus with atomic mass number A rises less strongly than linearly with A. This effect is known as shadowing. The experimental quantity which is usually considered in this context is the ratio of the per-nucleon cross sections on a nucleus (A) and on a deuteron (D)

$$R^{\mathrm{A}} = \frac{\sigma_{\mathrm{A}}/\mathrm{A}}{\sigma_{\mathrm{D}}/2}. \qquad (1)$$

The ratio R^{A} measures the shadowing effect on a nucleus relative to that on the deuteron. Information on nuclear shadowing in the deuteron may be obtained from measurements of the μ proton to μ deuteron cross section ratio [4, 5].

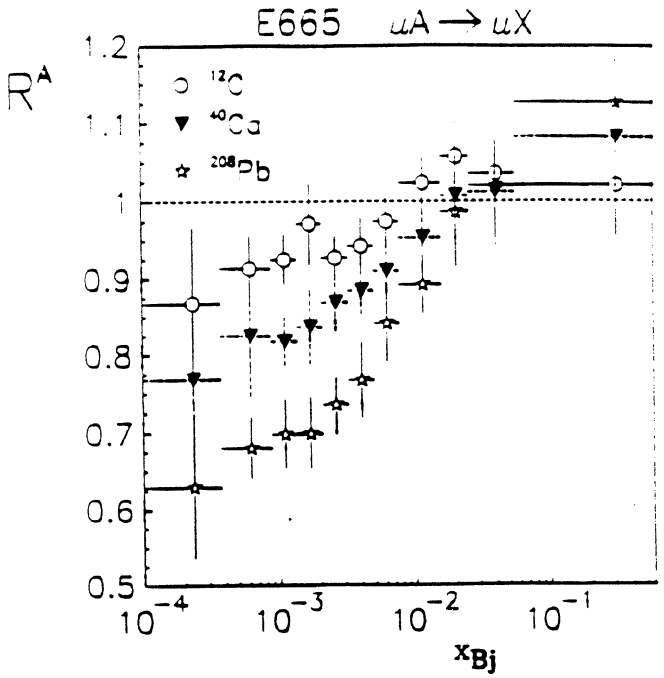

Figure 1. The shadowing ratio R^A plotted as a function of x_{Bj} for the C, Ca and Pb target.

In this analysis R^A is measured for C, Ca and Pb nuclei [6, 7]. Only events satisfying the criteria

$$Q^2 > 0.1 \text{ GeV}^2,\ \nu > 50 \text{ GeV},\ y < 0.7,\ E_{cl}/\nu < 0.21$$

were considered. Q^2 denotes the negative square of the four-momentum of the virtual photon, ν is the laboratory energy of the virtual photon, $y = \nu/E_{\text{beam}}$ (E_{beam} = laboratory energy of the incident muon) and E_{cl} the energy contained in the highest-energy cluster detected in the electromagnetic calorimeter. The Q^2 and ν cuts remove non-interacting beam particles and events with poor resolution in the kinematic quantities. The y cut excludes the region where radiative effects are predominant. Finally the E_{cl}/ν cut was applied to remove the dominant A-dependent radiative background (coherent and quasi-elastic muon bremsstrahlung and elastic muon-electron scatters). It was estimated that the E_{cl}/ν cut rejected $\sim$ 17% of the inelastic non-radiative events (indepedently of A) while removing practically all of the coherent, quasi-elastic muon bremsstrahlung and μ-e elastic events. If, alternatively to the E_{cl}/ν cut, radiative effects were corrected for using a method based on calculations by Mo and Tsai [8, 9] the ratio R^A was found to be systematically lower by 2 to 8%.

The use of a target cycling system greatly reduced the systematic uncertainties due to time dependent detector response. Systematic uncertainties on R^A were determined by varying the above cuts within wide ranges and by varying details of the analysis procedure. The systematic error due to the kinematic cuts is estimated as 4%, due to radiative background as less than 5%. There is an additional systematic error of less than 1.55% due to uncertainties in the relative normalisation of the cross section on a nucleus and on the deuteron.

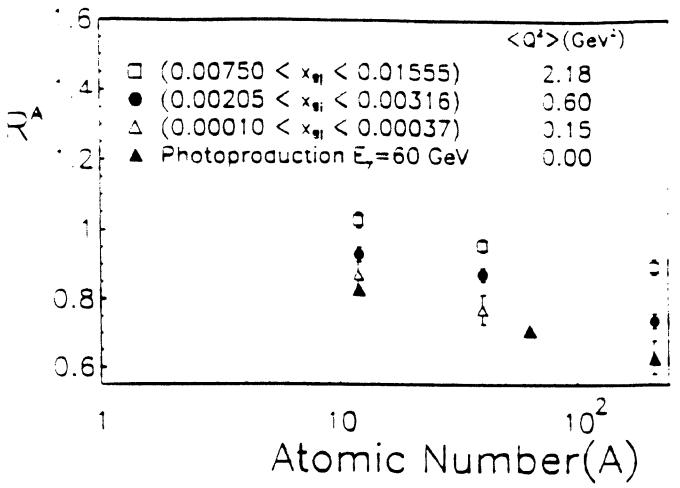

Figure 2. A dependence of the shadowing ratio R^A for three selected bins of x_{Bj}. For each x_{Bj} bin the average Q^2 is given. Shadowing data from a photoproduction experiment at a photon energy of 60 GeV [10] are shown for comparison.

The measurements of R^A are shown for the various targets as a function of x_{Bj} in figure 1. Nuclear shadowing ($R^A < 1$) is seen for all targets in the region $x_{Bj} \lesssim 0.01$, with a strong dependence on x_{Bj} and A. In figure 2 R^A is plotted for three selected x_{Bj} bins as a function of A, and compared with R^A from a photoproduction experiment [10]. As x_{Bj}, and thus also Q^2, decreases both the A dependence and the size of R^A approach the photoproduction measurements.

Within the experimental errors, no significant dependence of R^A on Q^2 or ν, at fixed x_{Bj}, is observed. For $x_{Bj} \lesssim 0.001$ the data from this analysis are compatible with the ν dependence of R^A for Cu as measured in a photoproduction experiment in the region ($20 < \nu < 185$ GeV) [10].

In summary, nuclear shadowing of the inelastic cross section is observed on the targets C, Ca and Pb relative to D in the region $x_{Bj} \lesssim 0.01$. The effect increases strongly with increasing A and decreasing x_{Bj}, approaching at the lowest x_{Bj} and Q^2 the photoproduction measurements. The data are consistent with no Q^2 or ν dependence at fixed x_{Bj}.

3. Diffractive scattering

In certain classes of models for nuclear shadowing there is a close relation between the cross section for diffractive scattering and the size of the shadowing effect [11]. The aim of the present analysis is to test this relation within a single experiment, by comparing nuclear shadowing

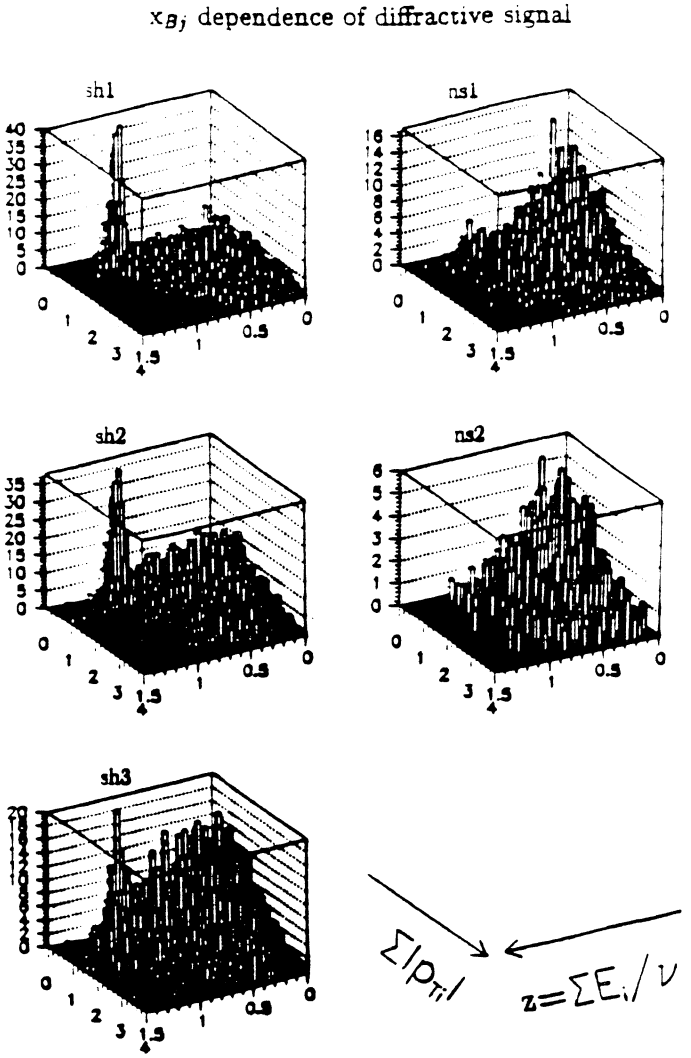

Figure 3. The number of events obtained on the Pb target plotted versus $\sum|p_{Ti}|$ and z, for five bins of x_{Bj}: sh1 = ($x_{Bj} < 0.002$), sh2 = ($0.002 < x_{Bj} < 0.0063$), sh3 = ($0.0063 < x_{Bj} < 0.02$), ns1 = ($0.02 < x_{Bj} < 0.063$) and ns2 = ($x_{Bj} > 0.063$). Clear diffractive signals are seen at $z \gtrsim 0.85$ and low $\sum|p_{Ti}|$, in those regions of x_{Bj} where also nuclear shadowing is observed.

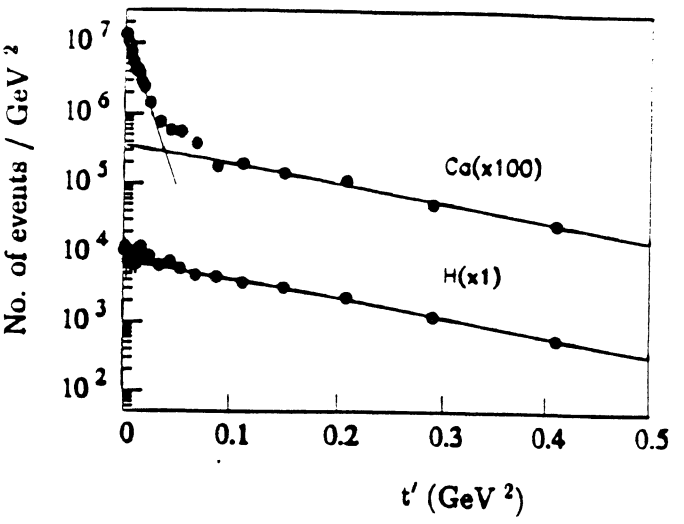

Figure 4. Distribution of $t' = t - t_{min}$ for diffractive production of $\rho(770)$ mesons on the proton and Ca target.

and diffractive scattering with respect to their A and x_{Bj} dependence. At present only preliminary and uncorrected data are available. However, already these data show interesting qualitative features which seem to support the expected close connection between nuclear shadowing and diffractive scattering.

The analysis starts from similar data samples as used for the shadowing analysis (Sect. 2), applying slightly different selection criteria: $Q^2 > 0.1$ GeV^2, $\nu > 20$ GeV, $y < 0.8$, $E_{cl}/\nu < 0.35$. In addition, only events with at least one positive and one negative hadron are accepted, resulting in ≈ 40000 events per target.

The hadronic center of mass system (cms) is defined as the system formed by the virtual photon and a target nucleon, which is assumed to be at rest in the laboratory frame. The detector has acceptance for charged particles travelling into the forward hemisphere of the cms, where "forward" is defined by the direction of the virtual photon. Transverse momenta will be defined relative to the direction of the virtual photon in the cms.

In order to establish the presence of diffractive events properties of a hadronic system X, formed by hadrons which are separated in rapidity from the target nucleon by more than 4.5 units, are investigated. Clear diffractive signals are seen in two-dimensional plots of the energy fraction z (carried by the system X) versus the charged multiplicity n_{ch}, the mass M, the transverse momentum p_T of the system X or versus $\sum|p_{Ti}|$ (see figure 3), the sum of the transverse momenta of *all* observed hadrons in the event. The diffractive events are characterized by z being close to 1 and by low values of n_{ch}, p_T, M and $\sum|p_{Ti}|$. The accumulation of events near $z \approx 1$ is considered as the main signature for diffractive events. Note that this signature is equivalent to requiring a large rapidity gap: if practically all of the available energy ($z \approx 1$) is going into a restricted region of rapidity, there is no energy left for hadrons to populate the remaining rapidity range (except for low momentum hadrons from the dissociation of the target).

Figure 3 shows z versus $\sum|p_{Ti}|$ for the Pb target, for five bins of x_{Bj}. There is a striking dependence on x_{Bj}: the diffractive signal dominates at the lowest x_{Bj}, decreases with increasing x_{Bj} and disappears in the x_{Bj} region where also nuclear shadowing was observed to vanish ($x_{Bj} \gtrsim 0.02$). This is a clear indication of the close relation between nuclear shadowing and diffractive scattering. The corresponding plots for the D

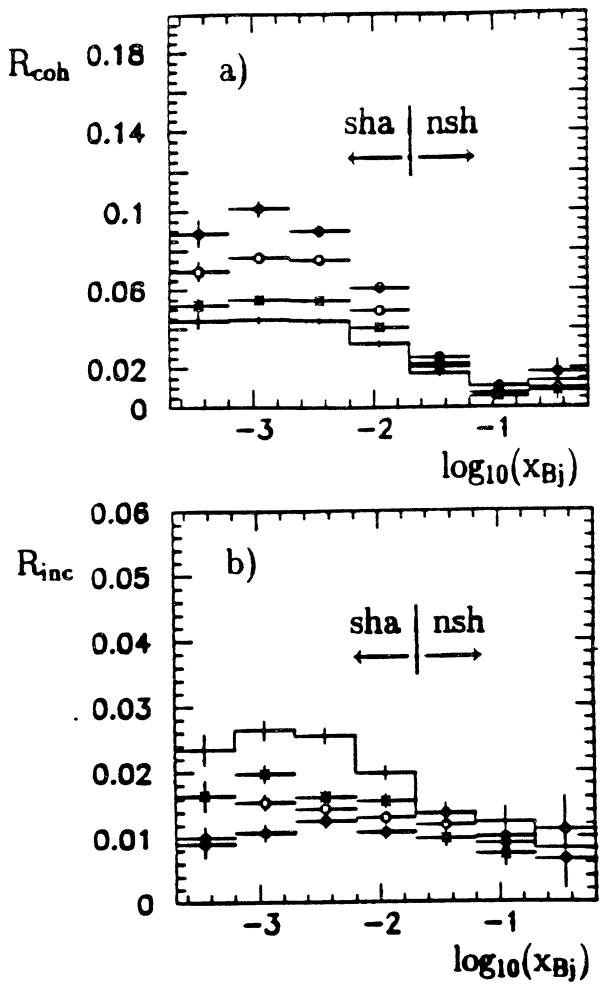

Figure 5. a) Ratio $R_{coh} = N^{coh,diff}/N^{all}$ of the number of coherent diffractive events and the number of all events as a function of x_{Bj}, for the targets D (−), C (∗), Ca (o) and Pb (•). The arrows indicate the regions, where nuclear shadowing of the inelastic cross section is observed (sha) or not observed (nsh). b) as a) but for the ratio $R_{inc} = N^{inc,diff}/N^{all}$ of the number of incoherent diffractive events and the number of all events.

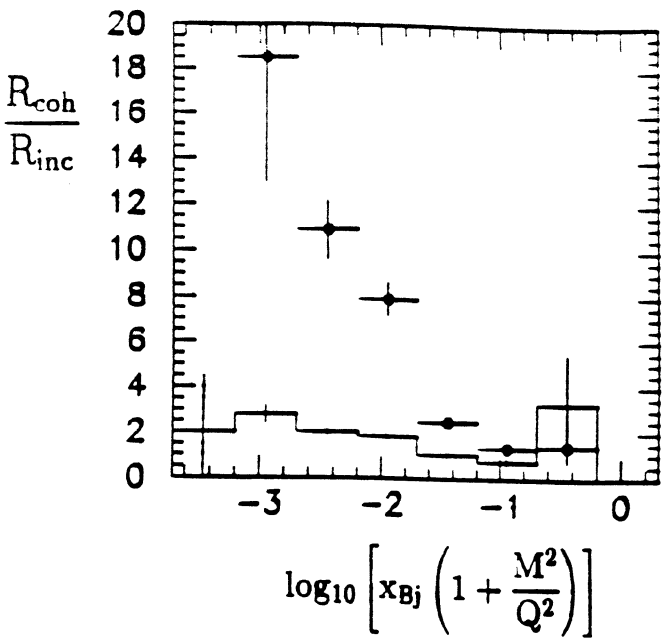

Figure 6. The ratio R_{coh}/R_{inc} as a function of $\kappa = x_{Bj}(1 + M^2/Q^2)$ for the D (−) and Pb (•) target.

target (not shown) exhibit the same qualitative features, except that the diffractive signals (relative to the non-diffractive background) are weaker than for the Pb target.

Due to the high resolution of the detector it is possible to identify two components of diffractive scattering: coherent and incoherent scattering. This is demonstrated in figure 4, in which the distribution of $t' = t - t_{min}$ for diffractive ρ production is displayed for the H and Ca targets. t is the negative four-momentum transfer squared from the virtual photon to the target. The two components are clearly visible in the case of Ca. In the following the events with an observed hadronic charge of zero and an energy fraction (carried by the system of all observed charged hadrons) greater than 0.85 are called diffractive. The additional selection $t' < 0.1$ GeV^2 defines the coherent diffractive, the selection $0.1 < t' < 1$ GeV^2 the incoherent diffractive sample. The exponential drop of the t' distributions (see figure 4) is another signature for diffractive scattering.

Figure 5 shows as a function of x_{Bj} the ratios R_{coh} and R_{inc} for the four targets D, C, Ca and Pb, where R_{coh} (R_{inc}) is the fraction of coherent (incoherent) diffractive events in the total event sample. There is a striking similarity between the x_{Bj} and A dependence of R_{coh} and that of the shadowing effect shown in figure 1: both increase with decreasing x_{Bj} and with increasing A. The main variation of R_{inc} is in the low x_{Bj} region too, however, R_{inc} clearly decreases with increasing A. This behaviour is in qualitative agreement with the theoretical expectation [12].

The different x_{Bj} dependence of R_{coh} and R_{inc} for a given target is probably a consequence of the nuclear form factor $G^2(M_N^2\kappa^2)$ in the expression for the coherent diffractive cross section ($\kappa = x_{Bj}(1+M^2/Q^2)$, M_N is the nucleon-mass). This has yet to be tested more quantitatively. The present data support this interpretation, insofar as R_{coh}/R_{inc} exhibits a much stronger dependence on κ (figure 6) than on x_{Bj} or Q^2 (figure 5). The presence of $G^2(M_N^2\kappa^2)$ implies also a suppression of large coherently produced diffractive masses as compared to the incoherently produced ones.

The distribution of the diffractive mass M is displayed in figure 7 for the coherent and incoherent diffractive events, for the D and Pb targets. In all cases there is clear evidence for diffractive production of $\rho(770)$ and of $\phi(1020)$. Comparing the shapes of the mass distributions one sees that for both the D and Pb target the high-mass tail ($M \gtrsim 2$ GeV) is suppressed

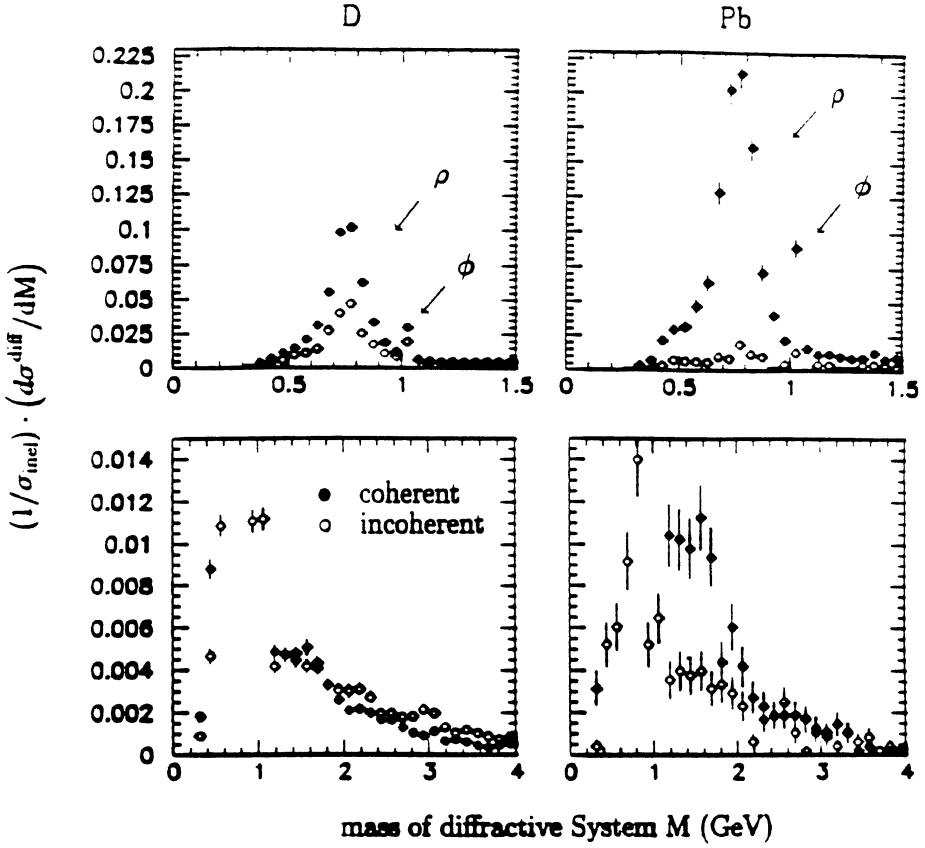

Figure 7. Distribution of the diffractive mass M (normalised to the number of inelastic events) in coherent and incoherent diffractive production on the D and Pb target. The scale in the two lower plots has been chosen such that the behaviour at higher masses is seen more clearly (the ρ and ϕ enhancements are partly cut off).

relative to the distribution below $M = 2$ GeV. The effect is much stronger for Pb than for D, as expected if it is due to the nuclear form factor. It should be noted that corrections for acceptance losses, which have not yet been applied, increase with increasing M. However, they are expected to affect the distributions for the coherent and incoherent events, and for the different targets, in a similar way.

The contributions from the different mass ranges (ρ, ϕ, $1.1 < M < 2$ GeV, $M > 2$ GeV) to the diffractive sample is plotted as a function of Q^2 in figure 8 for the D data. The trend of the data is similar for coherent and incoherent production, the higher masses being suppressed in the coherent sample relative to the incoherent sample. For $Q^2 \gtrsim 1$ GeV^2 there is a clear decrease with increasing Q^2 of the contribution from masses below 1.1 GeV (including the ϕ meson), which is compensated by an opposite behaviour of the masses above 1.1 GeV. This implies in particular an increase with Q^2 of the ρ'/ρ ratio, where the mass region between 1.1 and 2 GeV is denoted as $\rho'(\rho(1450)$ and $\rho(1700))$ [13, 14, 15].

In summary, the cross section for coherent diffractive scattering and the shadowing effect are found to have a qualitative similar dependence on A and x_{Bj}, both vanishing in the limit of low A or high x_{Bj}. This suggests a close relation between the two, as expected theoretically. In the kinematic region of the present experiment the diffractive cross section is dominated by $\rho(770)$ production. The $\rho'/\rho(770)$ ratio in diffractive production on deuterium increases with increasing Q^2.

4. A-dependence of diffractive ρ production

As has been shown in the previous section the dominant contribution to the diffractive cross section in the present experiment is due to exclusive prodution of $\rho(770)$. The A and Q^2 dependence of the cross section for exclusive ρ production is of particular interest as it may provide a test of the concept of color transparency [16, 17, 18].

At low x_{Bj} and high ν values exclusive production of ρ mesons may be visualised as follows. The virtual photon converts into a $q\bar{q}$ pair long before the nucleon is hit. The relevant length is the coherence length $l_c = 2\nu/(Q^2 + m_\rho^2)$, which is ≈ 107 fm at $x_{Bj} = 10^{-3}$. The $q\bar{q}$ pair interacts with the nucleons of the nucleus and recombines into the ρ meson after a length (formation

length) $l_f = \nu/(m_p \Delta m)$, where Δm is the typical level splitting of vector meson states. At high ν l_f greatly exceeds the size of the nucleus, therefore the transverse size of the $q\bar{q}$ pair does not change while passing through the nucleus. At a given Q^2 the dominant contribution to the cross section $\sigma_{q\bar{q}}$ on a nucleon comes from $q\bar{q}$ states with transverse size $\Delta x_T \sim 1/Q$. $\sigma_{q\bar{q}}$ as a cross section of a colorless object is proportional to Δx_T^2 and vanishes in the limit $\Delta x_T \to 0$.

The latter behaviour (called 'color transparency') may be tested by measuring the Q^2 and A dependence of the ρ production cross section: The size of the $q\bar{q}$ pair, and thus also $\sigma_{q\bar{q}}$ and the attenuation in a nucleus, are controlled by the value of Q^2. Due to color transparency the attenuation should decrease as Q^2 increases and vanish in the limit $Q^2 \to \infty$.

The events included in this analysis [19] are required to satisfy the following criteria:

- the event has exactly two oppositely charged hadrons (the decay pions of the ρ meson)
- the energy fraction ($\sum E_i/\nu$) carried by the hadrons must be consistent with 1 within 1.5 standard deviations
- $Q^2 > 0.1$ GeV^2, $\nu > 20$ GeV, $y < 0.7$
- $0.1 \leq t' = t - t_{min} < 0.8$ GeV^2 (selection of incoherent events)
- the effective mass $m_{\pi\pi}$ of the two hadrons, if they are assumed to be pions, has to be lower than 1.5 GeV (selection of ρ mesons)
- the effective mass m_{KK} of the two hadrons, if they are assumed to be kaons, has to be greater than 1.05 GeV (exclusion of ϕ mesons)

The events selected in this way show a Breit-Wigner-distribution of the ρ, with very little background [19]. The data were corrected for backgrounds from non-diffractive and coherent diffractive ρ production, and for losses due to the applied cuts.

The slope b of the t' distributions ($dN/dt' \sim \exp(-bt')$) is found to be $\sim$ 6.2 GeV^{-2} for all targets, a value characteristic for incoherent diffractive production.

In figure 9a the transparency T is displayed as a function of A for three bins of Q^2. T is defined as $\sigma_A/(A \cdot \sigma_0)$, where σ_A is the cross section on the nucleus and σ_0 is an estimate of the cross section on protons. Attenuation of the cross section ($T < 1$) is observed for all nuclear targets, with an approximately exponential dependence on A ($T \sim A^{\alpha-1}$). However, for all nuclear targets, T increases with increasing Q^2, which can be seen from the increase of α with Q^2 (figure 9b). This behaviour has been interpreted as possible evidence for the onset of color transparency [17, 18].

For the interpretation of the measurements on T it is of interest how l_c and l_f change with Q^2. For the

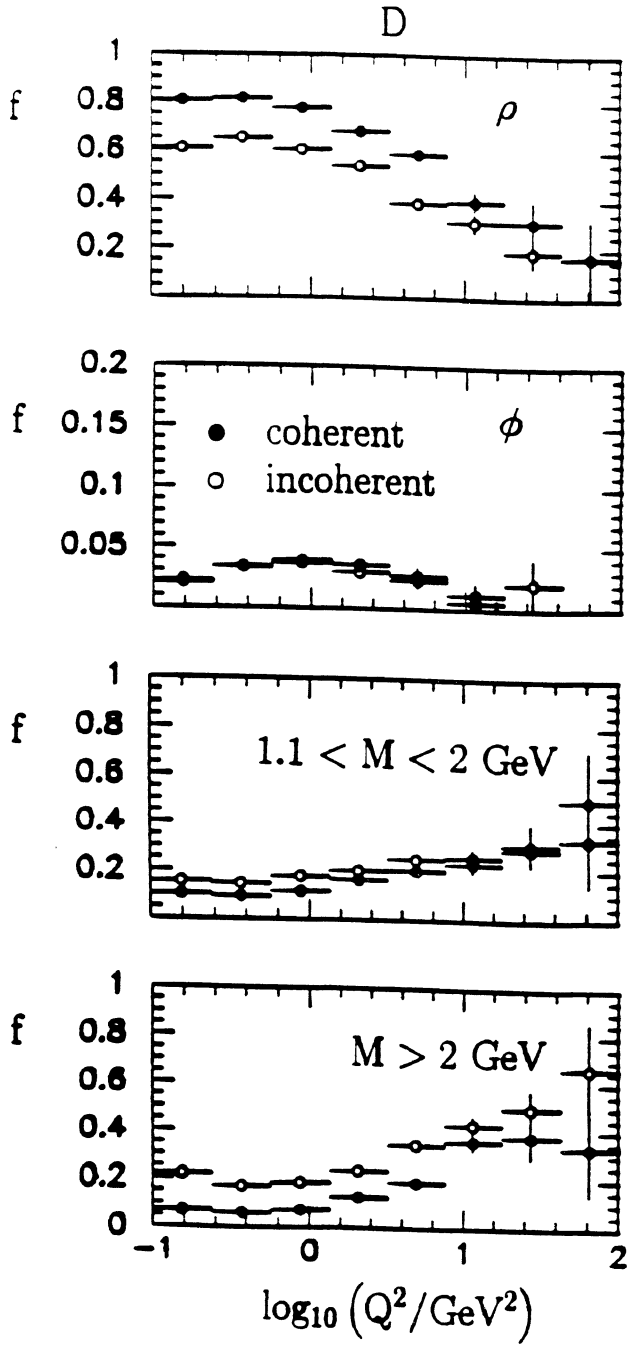

Figure 8. Contributions f to the coherent (incoherent) diffractive sample from a) the $\rho(770)$, b) the $\phi(1020)$, c) diffractive masses between 1.1 and 2 GeV (ρ' region) and d) diffractive masses above 2 GeV, plotted as a function of Q^2 for the D data.

three Q^2 bins chosen in figure 9 the average values of Q^2 are 0.212, 1.08 and 5.24 GeV^2, of x_{Bj} 0.0016, 0.0069 and 0.0330, of ν 144, 115 and 122 GeV, corresponding to $\langle l_c \rangle$ of 35, 20 and 6 fm, with $\langle l_f \rangle$ always being in the order of 30 fm. The nuclear radii r_A are 1.4, 2.5, 3.8 and 6.5 fm for D, C, Ca and Pb respectively. Thus the conditions $\langle l_c \rangle > r_A$, $\langle l_f \rangle > r_A$ are well fulfilled for the first two Q^2 bins and for all targets, whereas in

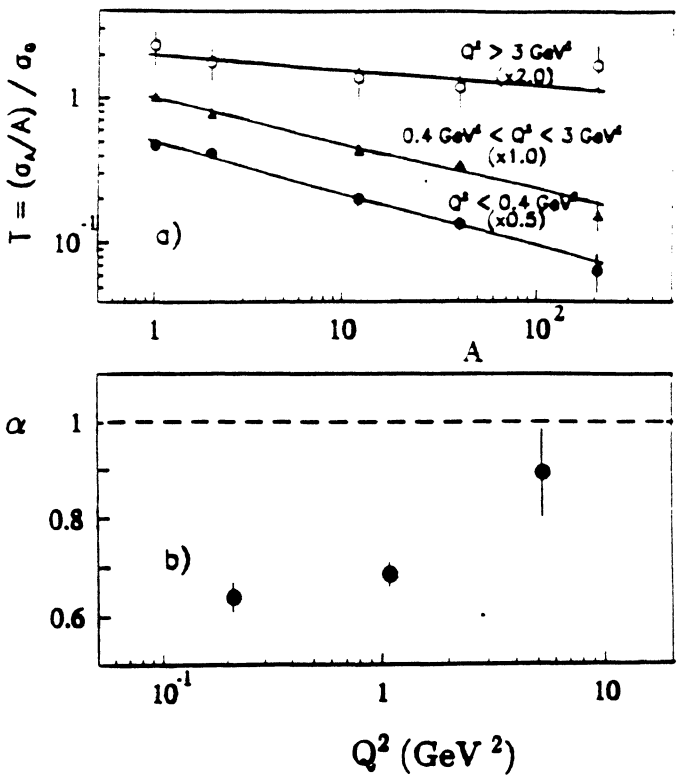

Figure 9. a) Nuclear transparency T for incoherent diffractive ρ production as a function of A for three bins of Q^2, b) Exponent α in the expresseion $T \sim A^{\alpha-1}$ versus Q^2, for incoherent diffractive ρ production.

the highest Q^2 bin $\langle l_c \rangle$ is in the order of the size of the nucleus for Ca and Pb.

It has yet to be clarified to which extent the increase of T in the region $3 < Q^2 < 10$ GeV^2 may be due to $\langle l_c \rangle$ becoming smaller than the size of the nucleus.

In conclusion, the per-nucleon cross section for incoherent diffractive production of $\rho(770)$ mesons on H, D, C, Ca and Pb has been measured as a function of Q^2. The nuclear transparency increases with increasing Q^2, which may indicate the onset of color transparency.

References

[1] M.R. Adams et al., Nucl. Instr. and Meth. A291 (1990) 533
[2] M. Arneodo et al., Phys. Rep. 240 (1994) 301
[3] M.R. Adams et al., Phys. Rev. Lett. 68 (1992) 3266
[4] M. Arneodo et al., Phys. Rev. D50 (1994) R1
[5] M.R. Adams et al., paper submitted to Phys. Rev. Lett. (1995)
[6] T.J. Carroll, Ph.D. thesis, University of Illinois at Chicago, 1994
[7] M.R. Adams et al., paper submitted to Z. Phys. C (1995)
[8] P. Amaudruz et al., Z. Phys. C51 (1991) 387
[9] L.W. Mo and Y.S. Tsai, Rev. of Mod. Phys. 41 (1968) 205; Y.S. Tsai, SLAC-PUB-848 (1971)
[10] D.O. Caldwell et al., Phys. Rev. Lett. 42 (1979) 553
[11] V.N. Gribov, Sov. Phys. JETP 29 (1969) 483
[12] N.N. Nikolaev et al., Z. Phys. A351 (1995) 435
[13] D. Aston et al., Nucl. Phys. B189 (1981) 15
[14] W.D. Shambroom et al., Phys. Rev. D26 (1982) 1
[15] T.J. Chapin et al., Phys. Rev. D31 (1985) 17
[16] S.J. Brodsky and A.H. Mueller, Phys. Lett. B206 (1988) 685
[17] B.Z. Kopeliovich at al., Phys. Lett. B324 (1994) 469
[18] S.J. Brodsky et al., Phys. Rev. D50 (1994) 3134
[19] M.R. Adams et al., Phys. Rev. Lett. 74 (1995) 1525